Distributed parameter control arithmetic for an axisymmetrical dual-mode scramjet

C. Tao, Y. Daren and B. Wen
Harbin Institute of Technology
Heilongjiang, China

ABSTRACT

Dual-mode scramjet is one of the candidates for hypersonic flight propulsion system which will be used in wide range of flight Mach numbers from 4 to 12 or higher, wherein dual-mode scramjet should be well designed to be suitable for subsonic/supersonic combustion operation according to the flight conditions. Therefore this system is required to operate in a finite number of operational modes that necessitate robust, stable, and smooth transitions between them by which selective operability of supersonic/subsonic combustion modes and efficient combustor operation in these modes may be realised. A key issue in making mode transition efficient and stable is mode transition control. The major problem in mode transition control is the handling of the various flow and combustion coupling effects of dual-mode scramjet whose physical states are spatially coupled and whose governing equations are partial differential equations. Involving these distributed parameter issues, our basic idea is using the shape control theory to study the control problems of mode transition for dual-mode scramjet with the aim of achieving the desirable design properties and increasing control reliabilities. This specific approach is motivated by the promise of novel techniques in control theory developed in recent years. Concrete control arithmetic of this approach, such as shape control model, sensitivity analysis and gradient-based optimisation procedure, are given in this paper. Simulation results for an axisymmetric, wall-injection dual-mode scramjet show the feasibility and validity of the method.

NOMENCLATURE

A	cross-sectional area
J	objective function
k	ratio of specific heats
M	Mach number
P	pressure
S	sensitivity
T	temperature
W	defined by Equation (20)
x	position co-ordinate along the axis of the channel
Z	defined by Equation (24)
τ	stagnation temperature rise ratio

Subscripts

2	isolator entry
3	combustor entry
4	nozzle entry
c	core flow
t	total
*	at the critical point

Paper No. 3256. Manuscript received 15 November 2007, revised 12 March 2008 accepted 9 May 2008.

1.0 INTRODUCTION

The development of dual-mode scramjet faces a number of technical challenges. Some of these challenges stem from the need to operate in a wide range of Mach numbers. The conflicting requirements of high cycle thermal efficiency and dissociation of the working fluid at excessively high static temperatures dictate that the combustion process must be subsonic (ramjet mode) for low Mach numbers, and supersonic (scramjet mode) for high Mach numbers[1]. Ramjet mode operation requires effective area distribution and tailored heat release profile to hold a stable choked thermal throat in the combustor, and also requires a guaranteed starting mechanism to ensure that the normal shock trains do not move upstream of the throat. Scramjet mode operation involves just weak oblique shock trains or shock free in the isolator. This results in small inlet losses and a clean profile at entry to the combustor. But it requires keeping the adverse pressure gradients small, and also requires decreasing the huge supersonic combustion loss (Rayleigh heating loss) by tailored heat release profile. As the flight passes through approximately Mach 5-6, the engine needs to transit from ramjet mode operation to scramjet mode operation.

Dual-mode scramjet operates in the ramjet/scramjet combustion modes, and they coordinate carefully tailored distribution of heat release and cross-sectional area in order to operate with both subsonic and supersonic combustion, and produce good thrust performance over a broad operation range[2]. Therefore it is important to control the feasible operation of dual-mode combustion systems and to control the transition between ramjet and scramjet modes in terms of fuel control procedures. This critical problem of matching heat release profile to combustor shape over a wide speed range has early been proposed in 1970s when Ferri[3] created the concepts that tailor the aerothermodynamics of fuel injection, mixing, and diffusive combustion to the desired engineering features of the fixed geometry dual-mode scramjet. But the challenges of engine design with assuring controlled heat release and avoiding strong inlet–combustor interactions, in a very demanding ground-test environment, make the timely achievement of such an undertaking very difficult indeed. Now these problems are still to some degree worrying the engine designers[4,5].

To help solving the problems of matching heat release profile to combustor shape, Ref. 6 has proposed the idea of distributed parameter control for dual-mode scramjet, and primary results have been presented. In this paper, the concrete distributed control arithmetic and simulation results will be further presented to make a clear introduction of the control arithmetic.

In the first part of this paper, the fundamental control problems of dual-mode scramjet will be again illuminated as presented in Ref. 6 to help understanding the whole distributed parameter control problem of dual-mode scramjet. In the second part, the shape control method is presented to solve the distributed parameter control problem. In the third part, a one-dimensional model for an axisymmetrical dual-mode scramjet is presented to be the shape control model. Finally, the key shape control procedures, such as sensitivity analysis and optimisation procedures are presented.

2.0 DISTRIBUTED PARAMETER CONTROL PROBLEMS OF DUAL-MODE SCRAMJET[6]

Because dual-mode scramjet is used under extreme temperatures and with wide range of Mach numbers, they show different control properties from other airbreathing engines, such as turbojet and ramjet engines.

As known, some turbojet and ramjet engines currently in production have yet used single-input single-output (SISO) controllers when having only fuel flow as the input variable and rotational speed as the output variable can have adequate controllers. For most modern turbojet and ramjet engines with variable geometry control in varied flight segments, a more complex control using multiple-input multiple-output (MIMO) techniques[7] has to be designed due to the strong interactions. The input variables include the main engine fuel flow and the nozzle area; variable geometry and afterburner fuel flow may also be the input variables in more complex engines. Parameters of interest for the controllers are the output variables. In order to use the important characteristics of the engines, the rotational speeds are selected as the output variable. Also other characteristic states variables can be taken such as the temperature and pressure of the intake, combustion chamber and compressor discharge[8]. These modern engines being multivariable in nature require more complicated control mechanisms and better control strategies for enhanced control over the variables to ensure improved performance of the plant[9]. Hence, new control techniques like linear feedback, optimal control, fuzzy control, sliding mode control etc, are being investigated in literatures. As from the above discussions, control technologies for the turbojet and ramjet engines are still in the frame of lumped parameter control where characteristic states variables can be found and chosen to represent the distributed parameter nature of the system by ordinary differential equations instead of partial differential equations. It is desirable to represent the physical system by a simplified mathematical model which describes only the significant characteristics of the system behavior. The control variables which have a major influence on the outputs and states are retained in the mathematical model; a lumped parameter control is then feasible[10].

But it's not certain for dual-mode scramjet if lumped parameter control can achieve the designate performance for the complex spatial interaction of the supersonic flow and supersonic combustion where the spatial effects can not be neglected[11]. Because dual-mode scramjets are such systems with obvious distributed parameter properties characterised by complex scramjet combustion and inlet-combustor interactions along the flow field. The flow field in a scramjet engine is transitional over a wide speed range, and in this range engine performance is characterised by complex transitional fluid dynamics, supersonic/subsonic flows with corresponding shock fields, coupled heat release/shock generation, combustion thermodynamics and chemical reactions[12]. So there are benefits from thinking scramjet engines through in terms of continuum mechanics with distributed parameter control. The detailed discussion on the distributed parameter control problem of scramjet engines has been presented in Ref. 6.

3.0 SHAPE CONTROL PROCEDURE TO REALISE DISTRIBUTED PARAMETER CONTROL OF DUAL-MODE SCRAMJET

The mathematical theories for distributed parameter control systems have been well-established due to the efforts of more than fifty years research by many well-known mathematicians and scientists. However, until recently the classic control tools for distributed parameter systems still rely on such complex mathematical techniques as fourier transforms, semi-group theory, sobolev spaces and etc[13]. The mathematical techniques of distributed parameter systems have been building from beginning of the fifty years on the basis of analytical theory of linear/nonlinear partial differential equations[14,15]. However, development during the last decades has shown serious limitations of these analytical methods, especially in evaluation of the dynamics of complex technological objects[16]. Therefore, in practical applications, numerical techniques, such as shape control techniques, are preferred for controlling such systems.

Shape control theory derives from structure optimisation techniques involving manipulating the structure's shape to conform to a desired shape specified by the designers. The notion of shape control was introduced into the journal literature through a

https://doi.org/10.1017/S0001924000002517 Published online by Cambridge University Press

contribution by Haftka and Adelman[17]. These authors presented the conception in particular regarding the shape control of space antenna, reflectors and etc so as to minimise the overall distortion of large space structures from their original shape. Applications range from controlling the shape of aerodynamic surfaces such as an aerofoil to large flexible space structures. Techniques of using shape control for smart structures were implemented by Balakrishnan[18] and Tan[19]. Agrawal and Treanor[20] employed the shape control algorithm to find the optimal actuator locations and voltages. Recently, Chee *et al*[21] considered more general error functions including curvatures and slopes and presented procedures to find the optimal voltage distribution in static shape control of smart plates based on numerical optimisation methods. Reference 22 deal with shape control by applied temperature. Murozono and Sumi[23] studied the active vibration control of a flexible cantilever beam by applying a transient thermal bending moment so that active control of the first bending mode is realised. Hsu *et al*[24] studied shape control of composite plates by bonded actuators with a high performance configuration. Moreover, applications of optimal shape theory in fluid mechanics include drag reduction[25], optimal sensor/actuator placement[26], airfoil design[27,28] and the design of wind tunnel elements[29].

The true shape control problem is a type of inverse problem with no explicit solutions. The core of shape control is to minimise the objective function usually defined as the squared difference of displacements between the desired and the actual shape. The most common approach to a shape control problem for a system governed by partial differential equations is to see the problem as a constrained nonlinear optimisation problem solved by the usual iterative methods of nonlinear optimisation, such as Newton or quasi-Newton methods. The method uses an objective function evaluation in the nonlinear optimisation procedure, and the evaluation of the gradient or Hessian of the objective function involves the solution of sensitivity equations for the partial differential equations considered.

Presently we consider the shape control of dual-mode scramjet as a one-dimensional steady control problem[6] aiming at control Mach number distribution (or pressure distribution). Control variables of the control system are the fuel flow rates in different fuel injections, which can be substituted by the equivalent variables: stagnation temperature rise ratio $\tau = [\tau_1, \tau_2, \cdots, \tau_m]$ where the subscript m denotes the number of fuel injections. The objective function is written as;

$$J(\tau) = \frac{1}{2}\int_{x_1}^{x_2}\left[\mathrm{M}(x,\tau) - \mathrm{M}_t(x)\right]^2 \mathrm{d}x \qquad \ldots (1)$$

where $\mathrm{M}_t(x)$ is the target shape, and $\mathrm{M}(x,\tau)$ is the feedback shape. Then the inverse control problem can be formulated as finding an optimal control variable τ^* to minimise this objective function. That is;

$$J(\tau^*) \le J(\tau) = \frac{1}{2}\int_{x_1}^{x_2}\left[\mathrm{M}(x,\tau) - \mathrm{M}_t(x)\right]^2 \mathrm{d}x \qquad \ldots (2)$$

Using gradient-based methods to solve the shape optimisation problems, one needs the gradient;

$$\nabla J(\tau_i) = \int_{x_1}^{x_2}\left[\mathrm{M}(x,\tau) - \mathrm{M}_t(x)\right]\frac{\partial}{\partial \tau_i}\mathrm{M}(x,\tau)\mathrm{d}x \qquad \ldots (3)$$

Note that the gradient involves both the state and the partial derivative of the state with respect to the control variable. This term is referred to as the sensitivity; henceforth, we use the following notation to denote the sensitivity;

$$S(x,\tau_i) = \frac{\partial}{\partial \tau_i}\mathrm{M}(x,\tau) \qquad \ldots (4)$$

In order to evaluate the objective function, the state $\mathrm{M}(x,\tau)$ must be computed. Hence the only additional work required for gradient evaluation is the computation of the sensitivity and forming the vector product in Equation (3). The gradient $\nabla J(\tau_i)$ can be calculated by computing the state and the sensitivity and then forming the inner product of the difference $[\mathrm{M}(x,\tau) - \mathrm{M}_t(x)]$ with the sensitivity.

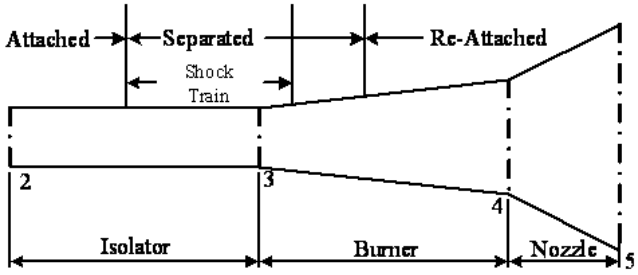

Figure 1. The axisymmetric, wall-injection dual-mode scramjet.

4.0 SHAPE CONTROL ARITHMETIC FOR AN AXISYMMETRICAL DUAL-MODE SCRAMJET

4.1 Shape control model

To give a primary proof on the idea of shape control for dual-mode scramjet, we choose the classic one-dimensional model of an axisymmetric, wall-injection dual-mode scramjet[30,31] as the shape control model. In the model, such physical phenomenon on inlet-combustor interaction as flow separation, shock trains and constant pressure heating are considered, as shown in Fig. 1.

For the case of frictionless flow without mass addition, but with change in both cross-sectional area A_c (subscript "c" represents the confined core flow) and total temperature T_t due to heat addition, the generalised one-dimensional flow equation for axial variation of Mach number is given by;

$$\frac{\mathrm{dM}}{\mathrm{d}x} = M\left(\frac{1+(k-1)\mathrm{M}^2/2}{1-\mathrm{M}^2}\right)\left\{-\left(\frac{1}{A_c}\frac{\mathrm{d}A_c}{\mathrm{d}x}\right) + \frac{1+k\mathrm{M}^2}{2}\left(\frac{1}{T_t}\frac{\mathrm{d}T_t}{\mathrm{d}x}\right)\right\} \qquad \ldots (5)$$

where $T_t(x)$ can be usefully represented in non-dimensional form by a rational function (ratio of polynomial functions) given by;

$$\tau(x) = 1 + (\tau - 1)\left\{\frac{\theta\chi}{1+(\theta-1)\chi}\right\}, \theta \ge 1 \qquad \ldots (6)$$

where $\tau(x) \equiv T_t(x)/T_{t2}$, $\chi \equiv (x - x_i)/(x_4 - x_i)$, x_i, is the axial location at which heat addition begins, θ is an empirical constant which depends on the mode of fuel injection and mixture.

4.1.1 In the ramjet mode operation

In ramjet mode, the flow must be subsonic at burner entry. Therefore the flow must be choked (M = 1) somewhere downstream, which causes a large back pressure p_3 at burner entry. This back pressure causes a normal shock train to form in the isolator. An asterisk "*" is used to designate the axial location of the chocked thermal throat, which is determined by;

$$-\left(\frac{1}{A_c}\frac{\mathrm{d}A_c}{\mathrm{d}x}\right) + \frac{(1+k)}{2}\left(\frac{1}{T_t}\frac{\mathrm{d}T_t}{\mathrm{d}x}\right) = 0 \qquad \ldots (7)$$

L'Hospital's rule can be used to evaluate Equation (5) at the choked thermal throat,

$$\left(\frac{\mathrm{dM}}{\mathrm{d}x}\right)_* = \frac{1}{4}\left\{-\Omega \pm \sqrt{\Omega^2 - 4\Psi}\right\} \qquad \ldots (8)$$

where;

https://doi.org/10.1017/S0001924000002517 Published online by Cambridge University Press

$$\Omega \equiv k\left(\frac{1}{A_c}\frac{\mathrm{d}A_c}{\mathrm{d}x}\right)_* \quad \ldots (9)$$

$$\Psi \equiv (k-1)\left(\frac{1}{A_c}\frac{\mathrm{d}A_c}{\mathrm{d}x}\right)_*^2 - (1+k)\left(\frac{1}{A_c}\frac{\mathrm{d}^2A_c}{\mathrm{d}x^2}\right)_* + \frac{(1+k)^2}{2}\left(\frac{1}{T_t}\frac{\mathrm{d}^2T_t}{\mathrm{d}x^2}\right)_* \quad \ldots (10)$$

To find the required subsonic entry Mach number, the ODE Equation (5) is solved for M(x) by marching upstream from x^* to x_3 and downstream from x^* to x_4, starting with M = 1 and choosing the positive-sign root for (dM/dx) in Equation (8).

The corresponding back pressure ratio p_3/p_2 of the normal shock train is determined by substituting M_3 into;

$$\frac{p_3}{p_2} = 1 + k\mathrm{M}_2^2 - k\mathrm{M}_2\mathrm{M}_3\sqrt{\left(1+\frac{k-1}{2}\mathrm{M}_2^2\right)\Big/\left(1+\frac{k-1}{2}\mathrm{M}_3^2\right)} \quad \ldots (11)$$

The length of the normal shock train is determined by;

$$L_s = \frac{\sqrt{\delta^{**}H}\left\{50(p_3/p_2-1)+170(p_3/p_2-1)^2\right\}}{\sqrt[4]{\mathrm{Re}\left(\mathrm{M}_2^2-1\right)}} \quad \ldots (12)$$

where Q^{**} is the inlet boundary layer momentum thickness, Re is the inlet Reynolds number, and H is the height of the isolator. This equation is obtained by experiment data[30].

4.1.2 In the scramjet mode operation with shock-free isolator

In the scramjet mode with shock-free isolator, there is no interaction between the burner and the isolator. As there is no pressure feedback from the burner, the aerothermodynamic state of the incoming flow is unaltered in the isolator. The calculation of axial variation of all properties within the burner is carried out by the direct marching solution of Equation (5).

4.1.3 In the scramjet mode operation with oblique shock train

In the scramjet mode with oblique shock train, the aerothermodynamic state of the combustion system is characterised by constant pressure combustion and oblique shock train in the isolator.

In the case of constant-pressure combustion, the axial variation of Mach number is given by;

$$\mathrm{M}(x) = \frac{\mathrm{M}_3}{\sqrt{\tau(x)\left(1+(k+1)/2\mathrm{M}_3^2\right)-(k+1)/2\mathrm{M}_3^2}} \quad \ldots (13)$$

The corresponding back pressure at the end of the oblique shock train equals to the maximum pressure in the burner. The Mach number at the end of the oblique shock train is obtained as;

$$\mathrm{M}_3 = \left\{\frac{k^2\mathrm{M}_2^2\left(1+(k-1)/2\mathrm{M}_2^2\right)}{\left(1+k\mathrm{M}_2^2-p_3/p_2\right)^2} - \left(\frac{k-1}{2}\right)\right\}^{-\frac{1}{2}} \quad \ldots (14)$$

and the length of the oblique shock train is determined by Equation (12).

Figures 2 and 3 show the simulation results of the shape control model, where the three classic combustion modes are calculated. The results are coincident with that in Ref. 30.

4.2 Sensitivity analysis

Sensitivities reflect the change trend of the shape (Mach number distribution), and they are needed in a gradient-based optimisation process in order to provide the gradients of the objective function. Sensitivity analysis are the most important part of the shape control arithmetic, especially for the nonlinear process of dual-mode scramjet. In this part, a key problem on the singularity of the sensitivity equation must be solved to assure the numerical stability of the arithmetic.

4.2.1 Sensitivity analysis in the ramjet mode operation

By the differential of Equation (5), we obtain the sensitivity equation;

$$\frac{\mathrm{d}}{\mathrm{d}x}S(x,\tau_i) = \left[-N_1\left(\frac{1}{A_c}\frac{\mathrm{d}A_c}{\mathrm{d}x}\right)+N_2\left(\frac{1}{T_t}\frac{\mathrm{d}T_t}{\mathrm{d}x}\right)\right]S(x,\tau_i) + N_3\frac{\partial}{\partial\tau_i}\left(\frac{1}{T_t}\frac{\mathrm{d}T_t}{\mathrm{d}x}\right) \quad \ldots (15)$$

where;

$$N_1 = \frac{2+(3k-1)\mathrm{M}^2-(k-1)\mathrm{M}^4}{2(\mathrm{M}^2-1)^2} \quad \ldots (16)$$

$$N_2 = \frac{2+(9k-1)\mathrm{M}^2+(5k^2-8k+1)\mathrm{M}^4-3k(k-1)\mathrm{M}^6}{4(\mathrm{M}^2-1)^2} \quad \ldots (17)$$

$$N_3 = \mathrm{M}\left(\frac{1+(k-1)\mathrm{M}^2/2}{1-\mathrm{M}^2}\right)\left(\frac{1+k\mathrm{M}^2}{2}\right) \quad \ldots (18)$$

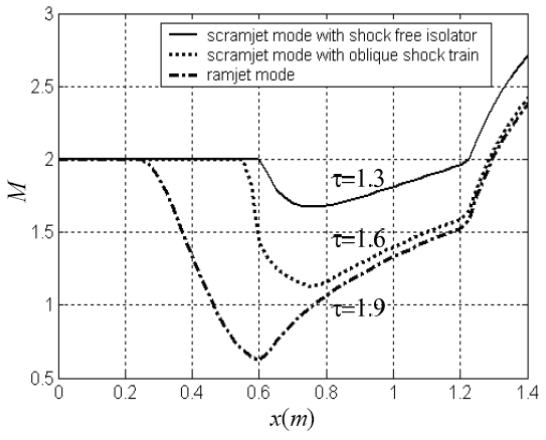

Figure 2. Calculated Mach number distribution of the shape control model.

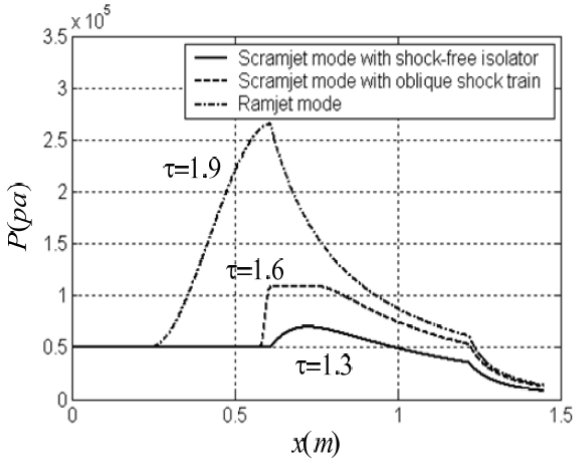

Figure 3. Calculated pressure distribution of the shape control model.

https://doi.org/10.1017/S0001924000002517 Published online by Cambridge University Press

It is important to observe that there is a marked difficulty in calculating the sensitivity equation involving singular problem about the choked thermal throat (M = 1), where the denominator "$(M^2 - 1)^2$" equals to zero. The singular problem will introduce high initial value error.

To solve this singular problem, we introduce a new solution method for the singular initial value problems of one-dimensional transonic flow in Equation (5). We change the form of Equation (5) into:

$$(1-\mathrm{M})\frac{\mathrm{dM}}{\mathrm{dx}}=\mathrm{M}\left(\frac{1+\frac{k-1}{2}\mathrm{M}^2}{1+\mathrm{M}}\right)\left\{-\left(\frac{1}{A_c}\frac{\mathrm{d}A_c}{\mathrm{dx}}\right)+\frac{1+k\mathrm{M}^2}{2}\left(\frac{1}{T_t}\frac{\mathrm{d}T_t}{\mathrm{dx}}\right)\right\} \quad \ldots (19)$$

where "(1 – M)dM/dx" can be written as $\mathrm{d}(-M^2 = 2M)/2$, from which a new variable can be defined as

$$W=-\mathrm{M}^2+2\mathrm{M} \quad \ldots (20)$$

Then the one-dimensional transonic flow equation of Equation (5) can be transformed into sectional equations.

(1) When M < 1

$$\frac{\mathrm{d}W}{\mathrm{dx}}=\left(\frac{\left(1-\sqrt{1-W}\right)\left[2+(k-1)\left(1-\sqrt{1-W}\right)^2\right]}{2-\sqrt{1-W}}\right)\left\{-\left(\frac{1}{A_c}\frac{\mathrm{d}A_c}{\mathrm{dx}}\right)+\frac{1+k\left(1-\sqrt{1-W}\right)^2}{2}\left(\frac{1}{T_t}\frac{\mathrm{d}T_t}{\mathrm{dx}}\right)\right\} \quad \ldots (21)$$

(2) When M = 1

$$W=1 \quad \ldots (22)$$

(3) When M > 1

$$\frac{\mathrm{d}W}{\mathrm{dx}}=\left(\frac{\left(1+\sqrt{1-W}\right)\left[2+(k-1)\left(1+\sqrt{1-W}\right)^2\right]}{2+\sqrt{1-W}}\right)\left\{-\left(\frac{1}{A_c}\frac{\mathrm{d}A_c}{\mathrm{dx}}\right)+\frac{1+k\left(1+\sqrt{1-W}\right)^2}{2}\left(\frac{1}{T_t}\frac{\mathrm{d}T_t}{\mathrm{dx}}\right)\right\} \quad \ldots (23)$$

Equations (21) ~ (23) show that the denominators of $2+\sqrt{1-W}$ and $2-\sqrt{1-W}$ equal to at the critical point where $W = 1$, and unequal to zero in the whole region. Therefore, the singularity of the transonic flow equation is eliminated.

After introducing the new variable W, the sensitivity may be redefined as;

$$Z(x,\tau)=\frac{\partial}{\partial\tau}W(x,\tau) \quad \ldots (24)$$

The corresponding sensitivity equation can be described as;

$$\frac{\mathrm{d}Z}{\mathrm{dx}}=\left\{-\frac{\partial N_1}{\partial W}\left(\frac{1}{A_c}\frac{\mathrm{d}A_c}{\mathrm{dx}}\right)+\frac{\partial N_2}{\partial W}\left(\frac{1}{T_t}\frac{\mathrm{d}T_t}{\mathrm{dx}}\right)\right\}Z+N_2\frac{\partial}{\partial\tau}\left(\frac{1}{T_t}\frac{\mathrm{d}T_t}{\mathrm{dx}}\right) \quad \ldots (25)$$

where

$$\frac{\partial}{\partial\tau}\left(\frac{1}{T_t}\frac{dT_t}{dx}\right)=\frac{\theta(x_4-x_3)}{[(\theta\tau-1)x-\theta\tau x_3+x_4]^2} \quad \ldots (26)$$

when M ≥ 1

$$N_1=\frac{2\left[1+\sqrt{1-W}\left[1+(k-1)/2\left[1+\sqrt{1-W}\right]^2\right]\right]}{2+\sqrt{1-W}} \quad \ldots (27)$$

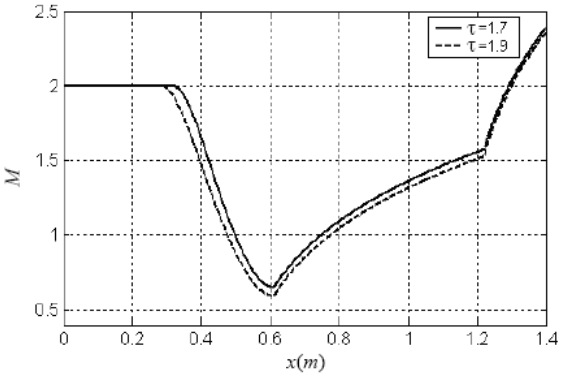

Figure 4. *M* distribution in the ramjet mode.

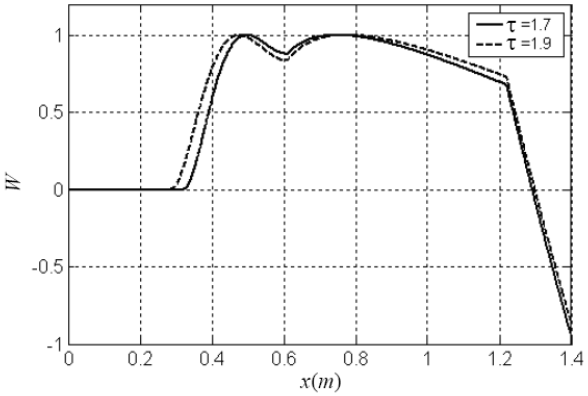

Figure 5. *W* distribution in the ramjet mode.

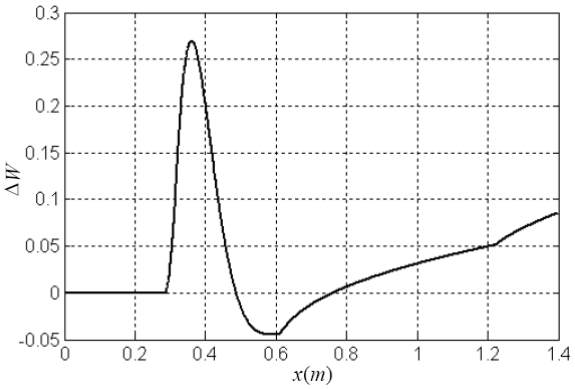

Figure 6. ΔW distribution in the ramjet mode.

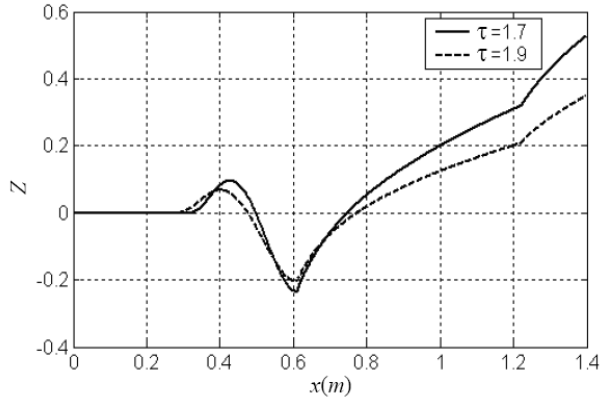

Figure 7. *Z* distribution in the ramjet mode

https://doi.org/10.1017/S0001924000002517 Published online by Cambridge University Press

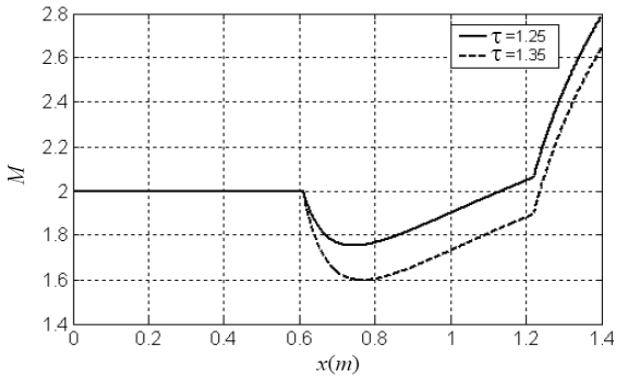

Figure 8. M distribution in the scramjet mode with shock-free isolator.

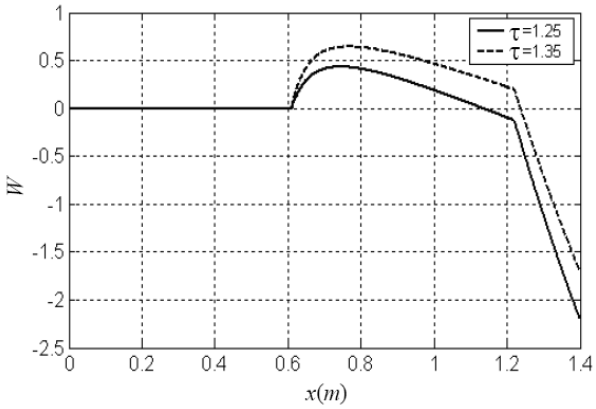

Figure 9. *W* distribution in the scramjet mode with shock-free isolator.

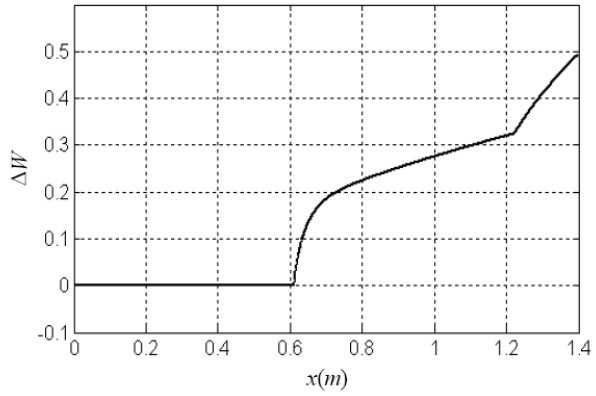

Figure 10. Δ*W* distribution in the scramjet mode with shock-free isolator.

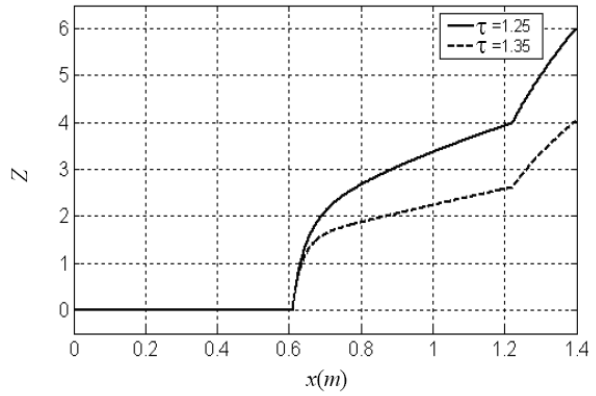

Figure 11. *Z* distribution in the scramjet mode with shock-free isolator.

and when M < 1

$$N_1 = \frac{2\left[1-\sqrt{1-W}\left[1+(k-1)/2\left[1-\sqrt{1-W}\right]^2\right]\right]}{2-\sqrt{1-W}} \quad \ldots (31)$$

$$N_2 = \left(\frac{2\left[1-\sqrt{1-W}\left[1+(k-1)/2\left[1-\sqrt{1-W}\right]^2\right]\right]}{2-\sqrt{1-W}}\right)\left(\frac{1+k\left[1-\sqrt{1-W}\right]^2}{2}\right) \quad \ldots (32)$$

$$\frac{\partial N_1}{\partial W} = -\frac{14-12/\sqrt{1-W}-\left[2-9/\sqrt{1-W}\right]W+k\left\{-14+14/\sqrt{1-W}+\left[2-9/\sqrt{1-W}\right]W\right\}}{-10+2W+8\sqrt{1-W}} \quad \ldots (33)$$

$$\frac{\partial N_2}{\partial W} = \frac{1}{4\left(-2+\sqrt{1-W}\right)^2\sqrt{1-W}}\left\{-12+(14-2W)\sqrt{1-W}-9W+k\left(62(-1+\sqrt{1-W})\right.\right.$$

$$\left.\left.+31(3-2\sqrt{1-W})W-\right.\right. \quad \ldots (34)$$

In the ramjet mode operation, the initial value condition to solve Eqs (25)~(34) is at the critical point, where;

$$Z(x^*) = 0 \quad \ldots (35)$$

Figure 4~7 show the sensitivity analysis results in the ramjet mode operation. Figures 4 and 5 show the Mach number distributions and the new variable *W* distributions along the *x*-axis with different stagnation temperature rise ratio τ of 1·7 and 1·9. Fig. 6 shows the change of W with τ of 1·7 and 1·9. Fig. 7 shows the distributions of the sensitivity function *Z* with τ of 1·7 and 1v9. As from the simulation results, we can see that the change trend of the sensitivity function *Z* along the *x*-axis is the same as that of Δ*W*. This means the simulation results of the sensitivity function is conceptually right as the definition of *Z* in Equation (24). Moreover, as shown in Fig. 7, the sensitivity functions with τ of 1·7 and 1·9 are different, which means the dual-mode combustion system is a nonlinear system.

4.2.2 Sensitivity analysis in the scramjet mode operation with shock-free isolator

In the scramjet mode with shock-free isolator, the aerothermodynamic state of the incoming flow is unaltered in the isolator, and there are no flow separations in the burner. Therefore, the calculation of axial variation of the sensitivity function within the burner is carried out by the direct marching solution of Equation (25), and the initial value condition is described as

$$Z_3 + Z_2 = 0 \quad \ldots (36)$$

Figures 8–11 show the sensitivity analysis results in the scramjet mode operation with shock-free isolator. Figures 8 and 9 show the Mach number distributions and the new variable *W* distributions along the *x*-axis with different stagnation temperature rise ratio τ of 1·25 and 1·35. Figure 10 shows the change of *W* with τ of 1·25 and 1·35. Figure 11 shows the distributions of the sensitivity function *Z* with τ of 1·25 and 1·35. As from the simulation results, we can see that the change trend of the sensitivity function *Z* along the *x*-axis is the same as that of Δ*W*. This means the simulation results in the scramjet mode operation with shock-free isolator is conceptually right.

4.2.3 Sensitivity analysis in the scramjet mode operation with oblique shock train

In the scramjet mode with oblique shock train, the aerothermodynamic state of the combustion system is characterised by constant pressure combustion and oblique shock train in the isolator.

In the case of constant-pressure combustion, the axial variation of

https://doi.org/10.1017/S0001924000002517 Published online by Cambridge University Press

W is given bv:

$$W(x)=\frac{-M_3^2+2M_3\sqrt{K_b+K_a\dfrac{T_t(x)}{T_{t0}}}}{K_b+K_a\dfrac{T_t(x)}{T_{t0}}} \quad \ldots (36)$$

Then we get the sensitivity function as

$$Z(x)=-\frac{K_aM_3\left(K_b+K_a\dfrac{T_t(x)}{T_{t0}}-M_3\sqrt{K_b+K_a\dfrac{T_t(x)}{T_{t0}}}\right)\dfrac{\partial}{\partial\tau}\left(\dfrac{T_t(x)}{T_{t0}}\right)}{\left(K_b+K_a\dfrac{T_t(x)}{T_{t0}}\right)^{5/2}} \quad \ldots (37)$$

where

$$K_a=1+\frac{k-1}{2}\mathrm{M}_3^2 \quad \ldots (38)$$

$$K_b=-\frac{k-1}{2}\mathrm{M}_3^2 \quad \ldots (39)$$

In the flow field where flow separation reattachs, the calculation of axial variation of the sensitivity function within the burner is carried out by the direct marching solution of Equation (25), and the initial value condition is obtained as;

$$Z(x_{reatt})=-\frac{K_aM_3\left(K_b+K_a\dfrac{T_t(x_{reatt})}{T_{t0}}-M_3\sqrt{K_b+K_a\dfrac{T_t(x_{reatt})}{T_{t0}}}\right)\dfrac{\partial}{\partial\tau_b}\left(\dfrac{T_t(x)}{T_{t0}}\right)\Big|_{x_{reatt}}}{\left(K_b+K_a\dfrac{T_t(x_{reatt})}{T_{t0}}\right)^{5/2}} \quad \ldots (40)$$

Figs. 12–15 show the sensitivity analysis results in the scramjet mode operation with oblique shock train. Figures 12 and 13 show the Mach number distributions and the new variable W distributions along the x-axis with different stagnation temperature rise ratio τ of 1·4 and 1·6. Figure 14 shows the change of W with τ of 1·4 and 1·6. Figure 15 shows the distributions of the sensitivity function Z with of 1·4 and 1·6. As from the simulation results, we can see that the change trend of the sensitivity function Z along the x-axis is the same as that of ΔW. This means the simulation results in the scramjet mode operation with oblique shock train is also conceptually right.

5.0 OPTIMISATION PROCEDURES

Gradient-based shape control procedure is a nonlinear optimisation problem and is computationally very expensive usually involving sensitivity function, gradient and Hessian evaluation. Gauss-Newton optimisation scheme is an efficient method for computing the nonlinear optimisation problem. The basis of the optimisation scheme is to approximate Hessian by neglecting the term that involves the second derivative of the residuals. Accordingly, we get;

$$\tau_i^{(k+1)}=\tau_i^{(k)}-\left[\nabla^2J(\tau_i^{(k)})\right]^{-1}\nabla J(\tau_i^{(k)}) \quad \ldots (41)$$

where

$$\tau_i^{(k+1)}=\tau_i^{(k)}-\left[\nabla^2J(\tau_i^{(k)})\right]^{-1}\nabla J(\tau_i^{(k)}) \quad \ldots (42)$$

$$\tau_i^{(k+1)}=\tau_i^{(k)}-\left[\nabla^2J(\tau_i^{(k)})\right]^{-1}\nabla J(\tau_i^{(k)}) \quad \ldots (43)$$

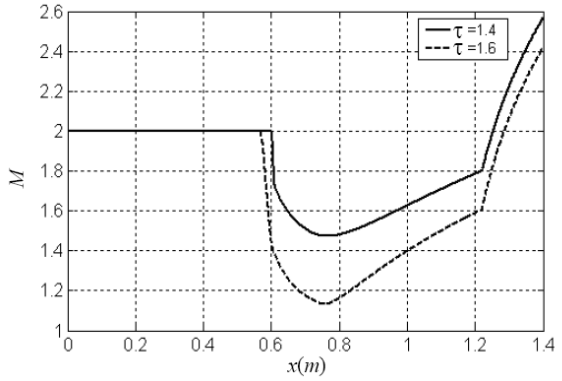

Figure 12. M distribution in the scramjet mode with oblique shock train.

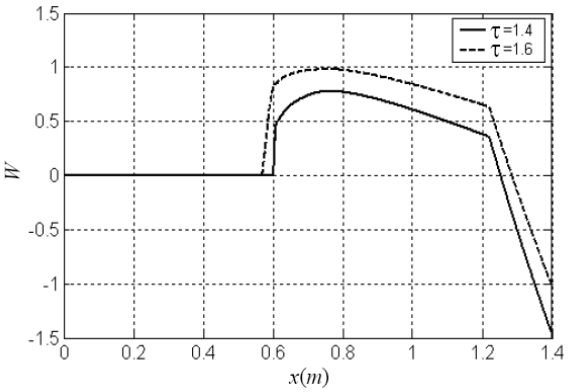

Figure 13. W distribution in the scramjet mode with oblique shock train.

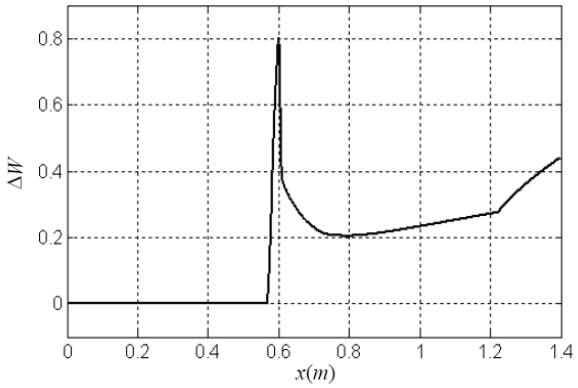

Figure 14. ΔW distribution in the scramjet mode with oblique shock train.

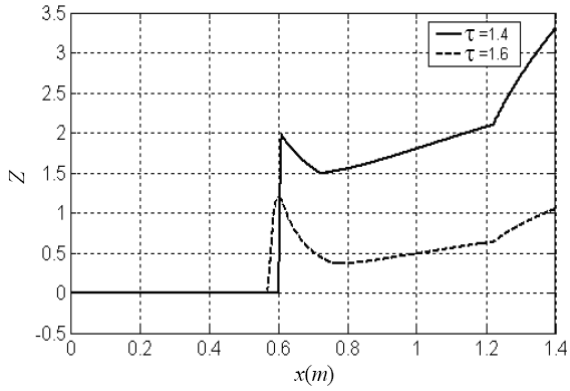

Figure 15. Z distribution in the scramjet mode with oblique shock train.

https://doi.org/10.1017/S0001924000002517 Published online by Cambridge University Press

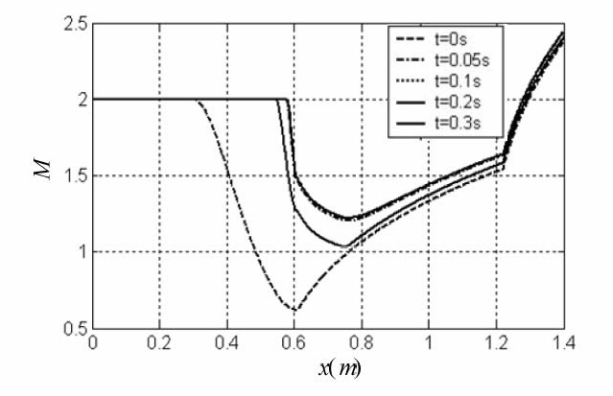

Figure 16. Distributed parameter control from ramjet mode to scramjet mode with oblique shock.

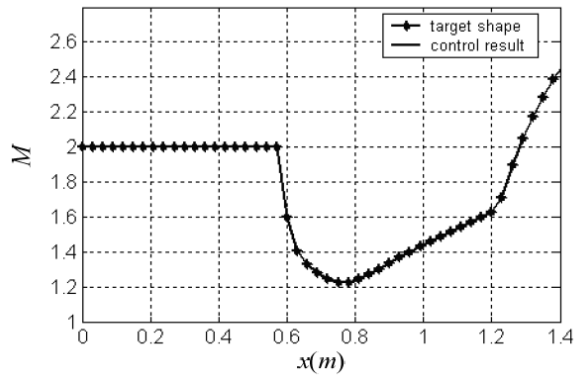

Figure 17. Comparison between the control result and the target shape.

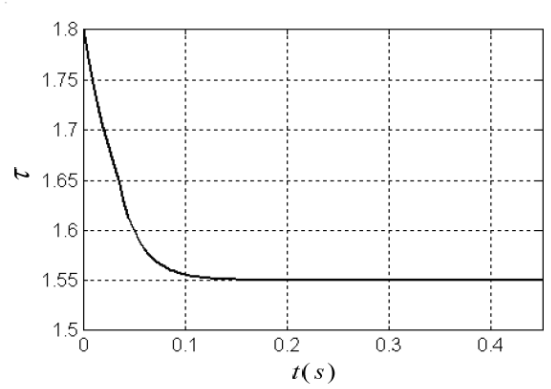

Figure 18. Change of control variable τ with time.

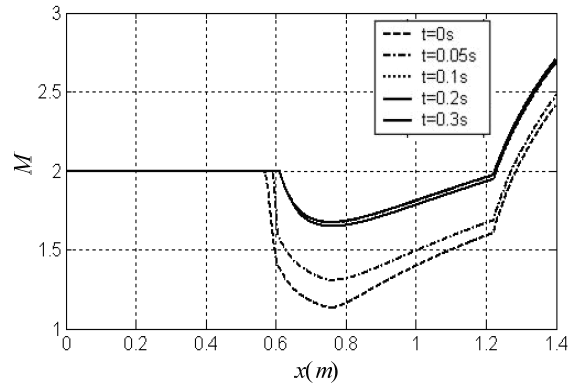

Figure 19. Distributed parameter control from scramjet mode with oblique shock to scramjet mode with shock-free isolator.

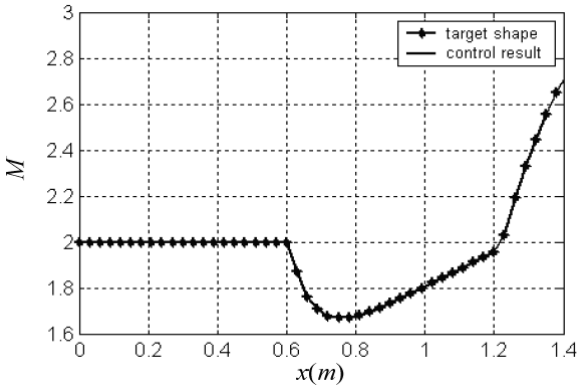

Figure 20. Comparison between the control result and the target shape.

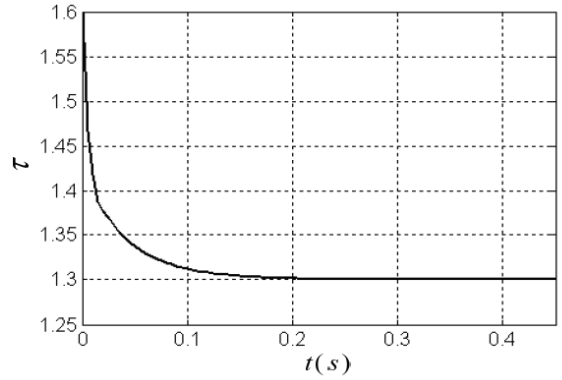

Figure 21. Change of control variable τ with time.

6.0 SIMULATION RESULTS

In this section, distributed parameter control will be simulated among ramjet mode, scramjet mode with oblique shock and scramjet mode with shock-free isolator with the shape control procedure. The number of fuel injections is currently considered as one. The actuator is selected as an inertial system modeled by $Y(s)/U(s) = 1/(Ls + 1)$, where L is the inertia time constant set by 0·05 rad/s, and the sampling time for the control system is set by 0·005s.

Firstly, distributed parameter control between ramjet mode and scramjet mode with oblique shock is simulated. The initial shape of Mach number distribution corresponds to the curve marked by "---" in Fig. 16, when the dual-mode scramjet operates in the ramjet mode and the initial stagnation temperature rise ratio τ_0 equals to 1.8. The target shape corresponds to the curve marked by "*" in Fig. 17 when the dual-mode scramjet operates in the scramjet mode with oblique shock and the appointed stagnation temperature rise ratio τ^* equals to 1·55. Figure 16 shows the distributed parameter control process by the shape control procedures. Figure 17 shows the comparison between the control result and the target shape. Figure 18 shows the changes of control variable τ with time respectively. According to simulation results, when t = 0·3s, τ = 1·5494, and the corresponding error is 0·04%. Secondly, distributed parameter control between scramjet mode with oblique shock and scramjet mode with shock-free isolator is simulated. The initial shape of Mach number distribution corresponds to the curve marked by "---" in Fig. 19, when the dual-mode scramjet operates in the scramjet mode with oblique shock and the initial stagnation temperature rise ratio equals to 1·55.

https://doi.org/10.1017/S0001924000002517 Published online by Cambridge University Press

The target shape corresponds to the curve marked by "*" in Fig. 20 when the dual-mode scramjet operates in the scramjet mode with shock-free isolator and the appointed stagnation temperature rise ratio τ^* equals to 1·30. Figure 19 shows the distributed parameter control process by the shape control procedures. Figure 20 shows the comparison between the control result and the target shape. Figure 21 shows the changes of control variable τ with time respectively. According to simulation results, when t = 0·3s, 1·3008, and the corresponding error is 0·06%. These simulation results mean that the shape control system is of high steady accuracy, also with high dynamic performance.

7.0 CONCLUSIONS

A method of distributed parameter control for dual-mode scramjet is proposed. The method is based on shape control theory to handle the control problem of the various flow and combustion coupling effects of dual-mode scramjet whose physical system is complex distributed parameter system. Concrete arithmetics of shape control, such as shape control model, sensitivity analysis and gradient-based optimisation procedure, are introduced in detail. Simulation results for an axisymmetric, wall-injection dual-mode scramjet show the validities of the shape control arithmetic with high steady accuracy and dynamic performance.

ACKNOWLEDGMENTS

The authors would like to thank Program for Outstanding Youth Foundation of Heilongjiang Province, China.

REFERENCES

1. DENIS, S.R. and KAU, H.P. Experimental study on transition between ramjet and scramjet modes in a dual-mode combustor, AIAA 2003-7048, December 2003.
2. EIJIRO, K. and TOHRU, M. Evaluating the aerodynamic performance of scramjet engines by pressure measurement, AIAA 2003-7053, December 2003.
3. EDWARD, T.C. Scramjet engines: The first forty years, *J Propulsion and Power*, 2001, **17**, (6), pp 1138-1148.
4. ALI, M., SADRUL, I. and AHMED, S. Mixing and flame holding with air inlet configuration in scramjet combustor, *International Communications in Heat and Mass Transfer*, 2004, **31**, (8), pp 1187-1198.
5. GRUBER, M.R., DONBAR, J.M. and CARTER, C.D. Mixing and combustion studies using cavity-based flameholders in a supersonic flow, *J Propulsion and Power*, 2004, **20**, (5), pp 769-778.
6. DAREN, Y., TAO, C. and WEN, B., An idea of distributed parameter control for scramjet engines, *Aeronaut J*, in press.
7. HAREFORS, M. Application of control structure design methods to a jet engine, *J Guidance, Control and Dynamics*, 2001, **24**, (3), pp 510-518.
8. HASHEM, A.A. and NADA, T.R. Design of turbofan engine controller based on non-linear analysis, *J Engineering and Applied Science*, 2002, **48**, (1), pp 137-153.
9. WANG, F., FAN, S.Q. and WU, D. Study of MAPS methods for turbofan engine performance seeking control, *J Aerospace Power*, 2005, **20**, (3), pp 503-507.
10. HOO, K.A. and ZHENG, D. Low-order control-relevant models for a class of distributed parameter systems, *Chemical Engineering Science*, 2001, **56**, (23), pp 6683-6710.
11. TOMIOKA, S., KOBAYASHI, K. and MURAKAMI, A. Distributed fuel injection for performance improvement of staged supersonic combustor, *J Propulsion and Power*, 2005, **21**, (4), pp 760-763.
12. GALLIMORE, S.D., JACOBSEN, L.S. and O'BRIEN, W.F. Operational sensitivities of an integrated scramjet ignition/fuel-injection system, *J Propulsion and Power*, 2003, **19**, (6), pp 183-189.
13. GODASI, S., KARAKAS, A. and PALAZOGLU, A. Control of nonlinear distributed parameter processes using symmetry groups and invariance conditions, *Computers and Chemical Engineering*, 2002, **26**, (7), pp 1023-1036.
14. HIRONOYI, A.F. Disrtibuted parameter approach to control large space structures, Proceeding of the 35th Conference on Decision and Control, Kobe, Japan, 1995.
15. KARLSSON, N. Optimal nonlinear distributed control of spatially-invariant systems, Proceeding of the 40th IEEE conference on decision and control, Orlando, Florida, USA, 2001.
16. YU, D.R., CUI, T. and BAO, W. Distributed parameter control method for hypersonic jets, *J Aerospace Power*, 2004, **19**, (2), pp 259-264.
17. HAFTKA, R.T. and ADELMAN, H.M. An analytical investigation of shape control of large space structures by applied temperatures, *AIAA J*, 1985, **23**, (45), pp 1-7.
18. BALAKRISHNAN, A.V. Shape control of plates with piezo actuators and collocated position/rate sensors, *Applied Mathematics and Computation*, 1994, **6**, (3), pp 213-234.
19. TAN, Z. Optimal linear quadratic gaussian digital control of an orbiting tethered antenna/reflector System, *J Guidance, Control and Dynamics*, 1994, **17**, (2), pp 234-241.
20. AGRAWAL, B.N. and TREANOR, K.E. Shape control of a beam using piezoelectric actuators, *Smart Materials and Structures*, 1999, **8**,(6), pp 729–739.
21. CHEE, C., TONG, L.Y. and STEVEN, G.P. Static shape control of composite plates using a slope-displacement-based algorithm, *AIAA J*, 2002, **40**, (8), pp 1611–1618.
22. IRSCHIK, H. and PICHLER, U. Dynamic shape control of solids and structures by thermal expansion strains, *J Thermal Stresses*, 2001, **24**, (3), pp 565–78.
23. MUROZONO, M. and SUMI, S. Active vibration control of a flexible cantilever beam by applying thermal bending moment, *J Intelligent Material and System Structure*, 1994, **5**, (4), pp 21–9.
24. HSU, C.Y., LIN, C.C. and GAUL, L. Shape control of composite plates by bonded actuators with high performance configuration, *J Reinforced Plastics Composition*, 1997, **16**, (18), pp 1692–710.
25. JOSYULA, E., PINNEY, M. and BLAKE, W.B. Applications of a counter flow drag reduction technique in high-speed systems, *J Spacecraft and Rockets*, 2002, **39**, (4), pp 605-614.
26. KIM, S.J. and SONG, K.Y. Active control of sound fields from plates in flow by piezoelectric sensor/actuator, *AIAA J*, 1999, **37**, (10), pp 1180-1186.
27. ELESHAKY, M.E. and BAYSAL, O. Airfoil shape optimization using sensitivity analysis on viscous flow equations, *J Fluids Engineering*, 1993, **115**, (1), pp 75-84.
28. ASHRAFIZADEH, A., RAITHBY, G.D. and STUBLEY, G.D. Direct design of airfoil shape with a prescribed surface pressure, *Numerical Heat Transfer*, 2004, **46**, (6), pp 505-527.
29. COCHRAN, L.S. and HOWELL, J.F., Wind tunnel studies for the aerodynamic shape for Sydney Australia, *J Wind Engineering and Industrial Aerodynamics*, 1990, **36**, (2), pp 801-810.
30. HEISER, W. and PRATT, D. Hypersonic airbreathing propulsion, *AIAA J*, Washington, D C, USA, 1994, pp 342-362.
31. TIMOTHY, F.O., RYAN, P.S. and MARK, J.L. Quasi-one-dimensional high-speed engine model with finite-rate chemistry, *J Propulsion and Power*, 2001, **17**, (6), pp 1366-1374.